Leading charm in hadron–nucleus interactions in the intrinsic charm model

T. Gutierrez , R. Vogt

Abstract

Leading charm hadrons produced in hadron–nucleus interactions cannot be adequately described within the parton fusion model. Recent results on charm baryon production in $\Sigma^- A$ interactions at 330 GeV with the WA89 detector disagree with fusion predictions. Intrinsic heavy quark pairs in the $\Sigma^-(dds)$ wavefunction provide a simple mechanism for producing fast charm hadrons. We calculate leading charm baryon production from Σ^-, π^- and p projectiles in a two component model combining parton fusion with intrinsic charm. Final state D^-, Σ_c^0, Ξ_c^+, and Λ_c^+ $d\sigma/dx_F$ distributions and D^-/D^+, D_s^-/D_s^+ and $\Lambda_c^+/\overline{\Lambda}_c^+$ asymmetries are compared to WA89 data. Predictions are made for 650 GeV $\Sigma^- A$ and $\pi^- A$ interactions in the SELEX detector at Fermilab and for 800 GeV pA interactions.

PACS: 12.38.Bx; 13.75.Ev; 14.20.Lg; 14.40.Lb

1. Introduction

One of the most striking features of charm hadroproduction is the leading particle effect: the strong correlation between the quantum numbers of the projectile and the final-state charm hadron. For example, more D^- than D^+ are produced at large x_F in $\pi^- A \to D^\pm X$ interactions [1–5]. Such correlations are remarkable because they explicitly contradict the perturbative QCD factorization theorem [6] which predicts that

heavy quarks hadronize through jet fragmentation functions independent of the initial state.

While leading charm effects are well established for D mesons, observations of charm baryons are more rare [7]. Two experiments with $\Sigma^-(dds)$ beams promise to clarify the situation in the baryon sector. The hyperon beam, with a strange valence quark, presents a unique opportunity to study the flavor dependence of leading charm hadroproduction since both charm and charm-strange baryons can be leading. The first, WA89, which directs a 330 GeV hyperon beam on carbon and copper targets, has reported the x_F distributions of $D^-(d\bar{c})$, $\Sigma_c^0(ddc)$, $\Xi_c^+(usc)$, and $\Lambda_c^+(udc)$ [8] as well as the D^-/D^+, D_s^-/D_s^+ and $\Lambda_c/\overline{\Lambda}_c$ production asymmetries [9]. The second, SELEX [10], has a large acceptance for forward charm production, enhancing the charm baryon yield. Their 650 GeV beam, approximately half $\pi^-(\bar{u}d)$ and Σ^-, promises to improve current samples from both beams by up to an order of magnitude. They also plan to study the A dependence of leading charm.

In previous work [11,12], a QCD mechanism which produces leading charm at large x_F was introduced. An important feature of the model is coalescence, the process through which a charm quark hadronizes by combining with quarks of similar rapidities, such as projectile spectator valence quarks. In a gauge theory the strongest attraction is expected to occur when the spectators and the produced quarks have equal velocities [13]. Thus the coalescence probability should be largest at small relative rapidity and rather low transverse momentum where the invariant mass of the $\overline{Q}q$ system is minimized, enhancing the binding amplitude.

This coalescence occurs in the initial state where the projectile wavefunctions of e.g. the π^-, p and Σ^- can fluctuate into Fock configurations containing a $c\bar{c}$ pair such as $|\bar{u}dc\bar{c}\rangle$, $|uudc\bar{c}\rangle$ or $|ddsc\bar{c}\rangle$ respectively. In these states, two or more gluons are attached to the charm quarks, reducing the amplitude by $\mathcal{O}(\alpha_s^2)$ relative to parton fusion [11]. The longest-lived fluctuations in states with invariant mass M have a lifetime of $\mathcal{O}(2P_{\rm lab}/M^2)$ in the target rest frame where $P_{\rm lab}$ is the projectile momentum. Since the comoving charm and valence quarks have the same rapidity in these states, the heavy quarks carry a large fraction of the projectile momentum and can thus readily combine to produce charm hadrons with large longitudinal momentum. Such a mechanism can then dominate the hadroproduction rate at large x_F. This is the underlying assumption of the intrinsic charm model [14] in which the wavefunction fluctuations are initially far off-shell. However, they materialize as charm hadrons when light spectator quarks in the projectile Fock state interacts with the target [15]. Since such interactions are strong, charm production will occur primarily on the front face of the nucleus in the case of a nuclear target. Thus the intrinsic charm mechanism has a stronger A dependence than charm production by leading-twist fusion.

In this work, we concentrate on the charm hadrons studied by WA89 and SELEX in order to further examine the relationship between fragmentation and coalescence mechanisms. The calculations are made within a two-component model: leading-twist fusion and intrinsic charm [11,12,16,17].

Leading particle correlations are also an integral part of the Monte Carlo program PYTHIA [18] based on the Lund string fragmentation model. In this model it is assumed that the heavy quarks are produced in the initial state with relatively small longitudinal momentum fractions by the leading-twist fusion processes. In order to produce a strong leading particle effect at large x_F, the string has to accelerate the heavy quark as it fragments into the final-state heavy hadron. Such a mechanism demands that large changes of the heavy quark momentum take place in the final state. Other models of leading charm production by recombination in the final state have been suggested [19,20]. However, in this work we will only compare our results with the commonly used PYTHIA Monte Carlo.

In this paper, we first discuss the conventional mechanism for charm production at leading-twist, parton fusion, and how the hyperon beam is taken into account in the model. Section 3 reviews the intrinsic charm model and describes the extension of the model used in this work. In Section 4 we compare our results on $\Sigma^- A$ interactions with the WA89 data and make predictions for SELEX with Σ^- and π^- beams as well as pA interactions. Finally, we summarize our results.

2. Leading-twist charm production

In this section we briefly review the conventional leading-twist model for the production of charm hadrons in $\Sigma^- p$, pp and $\pi^- p$ interactions. In leading-twist QCD, heavy quarks are produced by the fusion subprocesses $gg \to Q\overline{Q}$ and $q\overline{q} \to Q\overline{Q}$. The factorization theorem [6] predicts that fragmentation is independent of the quantum numbers of both the projectile and target. We will also show the corresponding distributions of charm hadrons predicted by the PYTHIA model [18].

Our calculations are at lowest order in α_s. A constant factor $K \sim 2$–3 is included in the fusion cross section since the next-to-leading order x_F distribution is larger than the leading-order distribution by an approximately constant factor [21]. An additional factor of two is included to obtain the single charm distribution, twice the $c\overline{c}$ cross section. Note that neither leading-order production nor the next-to-leading-order corrections can produce flavor correlations [22] such as those observed in leading charm production.

The charm hadron x_F distribution, where $x_F = (2m_T/\sqrt{s})\sinh y$, has the factorized form [17]

$$\frac{d\sigma}{dx_F} = \frac{\sqrt{s}}{2} x_a x_b \int H_{AB}(x_a, x_b) \frac{1}{E_1} \frac{D_{H/c}(z_3)}{z_3} dz_3\, dy_2\, dp_T^2 , \tag{1}$$

where a and b are the initial partons, 1 and 2 are the produced charm quarks with $m_c = 1.5$ GeV, and 3 and 4 are the final-state charm hadrons. The convolution of the subprocess cross sections for $q\overline{q}$ annihilation and gluon fusion with the parton densities is included in $H_{AB}(x_a, x_b)$,

$$H_{AB}(x_a, x_b) = \sum_q [\, f_q^A(x_a) f_{\bar{q}}^B(x_b) + f_{\bar{q}}^A(x_a) f_q^B(x_b)\,] \frac{d\hat{\sigma}_{q\bar{q}}}{d\hat{t}}$$

$$+ f_g^A(x_a) f_g^B(x_b) \frac{d\hat{\sigma}_{gg}}{d\hat{t}}\,, \tag{2}$$

where A and B are the interacting hadrons and the scale dependence of the parton densities has been suppressed. The subprocess cross sections can be found in Ref. [23]. Since we study $c\bar{c}$ production with several different projectiles, we specify the general $q\bar{q}$ convolution for three light flavors:

$$\sum_q [\, f_q^A(x_a) f_{\bar{q}}^B(x_b) + f_{\bar{q}}^A(x_a) f_q^B(x_b)\,] = u^A(x_a)\bar{u}^B(x_b) + \bar{u}^A(x_a)u^B(x_b)$$

$$+ d^A(x_a)\bar{d}^B(x_b) + \bar{d}^A(x_a)d^B(x_b) + s^A(x_a)\bar{s}^B(x_b) + \bar{s}^A(x_a)s^B(x_b). \tag{3}$$

Parton distributions of the hyperon are not available. However, using baryon number and momentum sum rules, a set of parton distributions for the Σ^- can be inferred from the proton distributions,

$$\int_0^1 u_v^p(x)\,dx = \int_0^1 d_v^{\Sigma^-}(x)\,dx = 2, \tag{4}$$

$$\int_0^1 d_v^p(x)\,dx = \int_0^1 s_v^{\Sigma^-}(x)\,dx = 1\,. \tag{5}$$

We also identify $s^p(x) = u^{\Sigma^-}(x)$. Similar relations can be made for the sea quarks. The gluon distributions are thus assumed to be the same in the Σ^- and the proton. Both the GRV LO 94 [24] and MRS D$^{-'}$ [25] parton distribution functions with $\bar{u} \neq \bar{d} \neq \bar{s}$ were used. Other, older distributions with a symmetric sea, $\bar{u} = \bar{d} = \bar{s}$, produce identical results for $\Sigma^- p$ and pp interactions.

The fragmentation functions, $D_{H/c}(z)$, describe the hadronization of the charm quark where $z = p_H/p_c$ is the fraction of the charm quark momentum carried by the charm hadron, assumed to be collinear to the charm quark. According to the factorization theorem, fragmentation is independent of the initial state and thus cannot produce flavor correlations, precluding a leading charm effect. This uncorrelated fragmentation will be modeled by two extremes: a delta function, $\delta(z-1)$, and the Peterson function [28], extracted from e^+e^- data. The Peterson function, derived from a non-hadronic initial state, predicts a softer x_F distribution than observed in hadroproduction, even at moderate x_F [17] since the fragmentation decelerates the charm quark. The parameters of the Peterson function we use here are taken from e^+e^- studies of D production [29]. Typically fits to charm baryon fragmentation functions suggest increased deceleration of the charm quark in final-state baryons relative to mesons. On the other hand, the delta-function assumes that the charm quark coalesces with a low-x spectator sea quark or a low momentum secondary quark with little or no momentum loss [17]. This

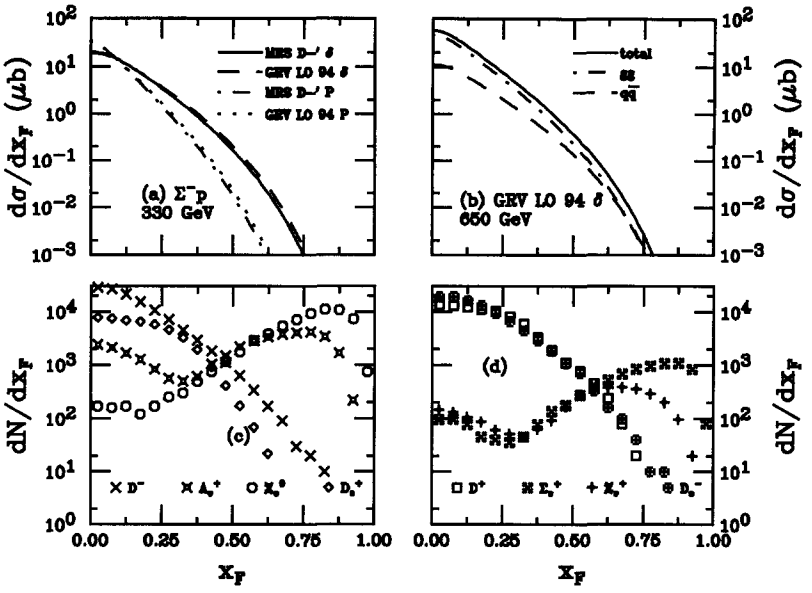

Fig. 1. Charm production by leading-twist fusion in $\Sigma^- p$ interactions. (a) Two parton distribution functions with two different fragmentation functions are shown at 330 GeV. The curves show calculations with the MRS D−′ parton distributions with delta function fragmentation (solid) and the Peterson function (dot-dashed) and with the GRV LO 94 parton distributions with delta function fragmentation (dashed) and the Peterson function (dotted). In (b) calculations with the GRV LO 94 parton distributions with delta function fragmentation are given at 650 GeV for the $q\bar{q}$ component (dashed), gg component (dot-dashed) and the total production cross section (solid). Charm hadron production in PYTHIA 6.115 at 330 GeV is shown in (c) and (d) with the distributions labeled as indicated.

assumption is more consistent with low p_T charm hadroproduction data [30–32] than Peterson fragmentation.

In Fig. 1a we show the inclusive x_F distributions calculated for both types of fragmentation in $\Sigma^- p$ interactions at 330 GeV. Both sets of parton distributions are also shown. Very little difference in either total cross section or shape of the x_F distributions can be discerned between the two sets of parton distributions. The delta function results in harder distributions than those predicted by Peterson fragmentation for $x_F > 0.2$. However, as shown in [8], even with this hard fragmentation the fusion model cannot account for the shape of leading charm baryon distributions. Fig. 1b shows the relative contributions from gg fusion and $q\bar{q}$ annihilation to the total cross section at 650 GeV, the energy of the SELEX beam, using the GRV LO 94 parton densities. Gluon fusion clearly dominates the production until $x_F \approx 0.6$. We have checked that this is also true at the lower energy of the WA89 experiment, 330 GeV.

We compare the $\Sigma^- p$ distributions with those from pp and $\pi^- p$ interactions at the same energies with our two choices of parton distributions in Figs. 2 and 3 respectively. Since the differences between the $\Sigma^- p$ and pp x_F distributions are rather small due to the dominance of gluon fusion, in Fig. 2a we show the ratio $\Sigma^- p/pp$ at 330 GeV. The differences between $\Sigma^- p$ and pp production are somewhat larger for the GRV LO 94

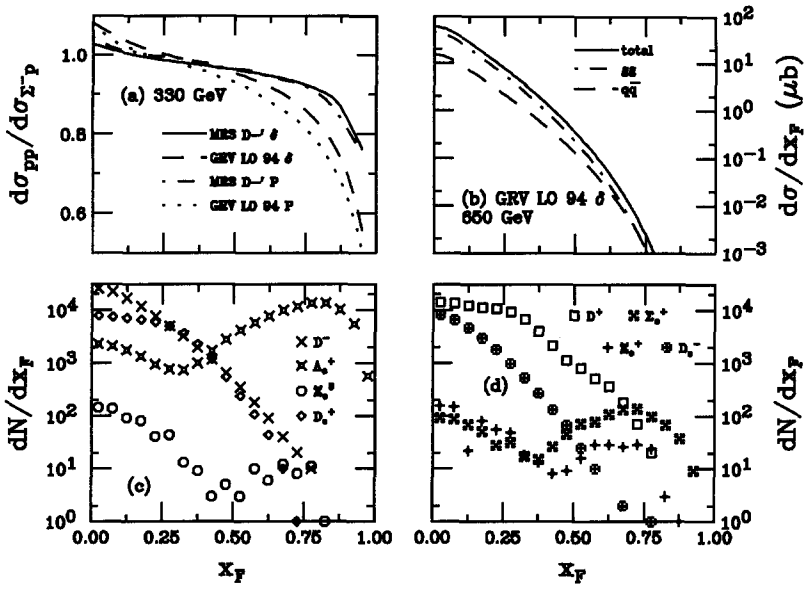

Fig. 2. Charm production by leading-twist fusion in pp interactions. (a) The cross section ratios $\sigma_{pp}/\sigma_{\Sigma^- p}$ are given for two parton distribution functions with two different fragmentation functions at 330 GeV. The curves show calculations with the MRS D$-'$ parton distributions with delta function fragmentation (solid) and the Peterson function (dot-dashed) and with the GRV LO 94 parton distributions with delta function fragmentation (dashed) and the Peterson function (dotted). In (b) calculations with the GRV LO 94 parton distributions with delta function fragmentation are given at 650 GeV for the $q\bar{q}$ component (dashed), gg component (dot-dashed) and the total production cross section (solid). Charm hadron production in PYTHIA 6.115 at 330 GeV is shown in (c) and (d) with the distributions labeled as indicated.

distributions than the MRS D$-'$, due to the relative assumptions of $\bar{u}/\bar{d}$. The GRV LO 94 set is based on more recent data than the MRS D$-'$ and should thus more accurately reflect the sea quark abundancies in the proton. In contrast, assumptions concerning charm quark fragmentation do not strongly affect the relative rates. In Fig. 2b we see that the relative $q\bar{q}$ contribution to pp production is somewhat larger at $x_F \approx 0$ than in $\Sigma^- p$ production at the same energy but this does not affect the point where gg fusion ceases to dominate $c\bar{c}$ production. The pion valence distributions are harder, allowing charm production at larger x_F than with a baryon beam, as shown in Fig. 3. For the pion, we use the GRV LO pion set [26] with the GRV LO 94 proton set and with the MRS D$-'$ distributions we use the SMRS P2 pion distributions [27]. However, the valence $\bar{u}$ quark in the π^- does not change the relative importance of $q\bar{q}$ annihilation at 650 GeV, as seen in Fig. 3b. Much lower energies are needed for the π^- antiquark to lead to dominance of $q\bar{q}$ annihilation in $c\bar{c}$ production.

The charm hadron distributions from PYTHIA 6.115 [18] for the three projectiles at 330 GeV beam energy are also shown in Figs. 1-3c,d. The PYTHIA calculations, based on 10^7 events, use all default program settings along with the GRV LO 94 parton distributions. We note that in PYTHIA the hyperon valence quark distributions are an average of the proton valence distributions, $d_v^\Sigma = s_v^\Sigma = (u_v^p + d_v^p)/3$. In Fig. 3c the D^-,

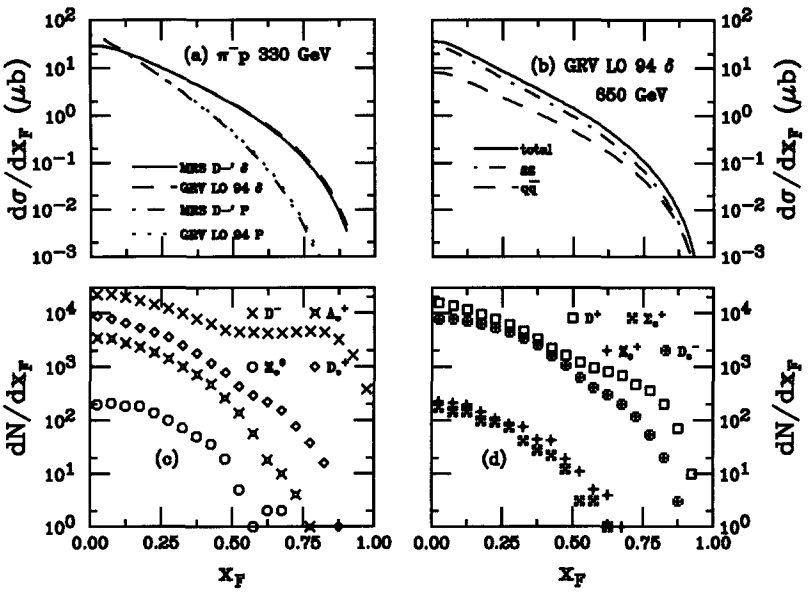

Fig. 3. Charm production by leading-twist fusion in $\pi^- p$ interactions. (a) Two parton distribution functions with two different fragmentation functions are shown at 330 GeV. The curves show calculations with the MRS D$-'$ parton distributions with delta function fragmentation (solid) and the Peterson function (dot-dashed) and with the GRV LO 94 parton distributions with delta function fragmentation (dashed) and the Peterson function (dotted). In (b) calculations with the GRV LO 94 parton distributions using delta function fragmentation are given at 650 GeV for the $q\bar{q}$ component (dashed), gg component (dot-dashed) and the total production cross section (solid). Charm hadron production in PYTHIA 6.115 at 330 GeV is shown in (c) and (d) with the distributions labeled as indicated.

D_s^+, Λ_c and Ξ_c^0 x_F distributions are shown while the D^+, D_s^-, Σ_c^0 and Ξ_c^+ distributions are given in Fig. 3d. The magnitude of the curves reflect the relative abundancies of charm hadrons produced by PYTHIA.

The Lund string fragmentation model [18] produces charm quarks at string endpoints. The strings pull the charm quarks toward the opposite endpoints, typically the beam remnants. When the two string endpoints are moving in the same general direction, the charm hadron can be produced with larger longitudinal momentum than the charm quark. In the case where the string invariant mass is too small for multiple particle production, a single hadron is produced [33], as in the $\Sigma_c^0(ddc)$ and $\Xi_c^0(dsc)$ which share two valence quarks with the Σ^-. These distributions have a minimum at $x_F \sim 0.3$ and 0.1 respectively and a peak at $x_F \sim 0.8$, illustrating the acceleration undergone by charm quarks by strings with small invariant mass. The Λ_c and Ξ_c^+ are also accelerated by string fragmentation but the effect is not as strong because only one valence quark is in common with the projectile.

In contrast, with a proton beam, as shown in Fig. 2, only the Λ_c shows strong forward acceleration due to the common u and d quarks with the maximum in the x_F distribution occurring at $x_F \approx 0.8$. A second peak is notable for the Σ_c^0 but the acceleration effect is weaker for charm-strange baryon production, presumably due to the additional mass

of the strange quark. While meson production does not show any significant leading behavior with a baryon projectile, the situation is reversed with the π^- beam where D and D_s production is clearly forward of all charm baryon production, produced centrally in the forward x_F region. We will make further comparisons with PYTHIA when our full model is discussed.

3. Intrinsic particle production

The wavefunction of a hadron in QCD can be represented as a superposition of Fock state fluctuations, e.g. $|n_V\rangle$, $|n_V g\rangle$, $|n_V Q\overline{Q}\rangle$, ... components where $n_V \equiv dds$ for a Σ^-, uud for a proton and $\overline{u}d$ for a π^-. When the projectile scatters in the target, the coherence of the Fock components is broken and the fluctuations can hadronize either by uncorrelated fragmentation as for leading-twist production or coalescence with spectator quarks in the wavefunction [14,15]. The intrinsic heavy quark Fock components are generated by virtual interactions such as $gg \to Q\overline{Q}$ where the gluons couple to two or more projectile valence quarks. The probability to produce $Q\overline{Q}$ fluctuations scales as $\alpha_s^2(M_{Q\overline{Q}})/m_Q^2$ relative to leading-twist production [34]. Intrinsic $Q\overline{Q}$ Fock states are dominated by configurations with equal rapidity constituents so that, unlike sea quarks generated from a single parton, the intrinsic heavy quarks carry a large fraction of the parent momentum [14].

The frame-independent probability distribution of an n–particle $c\overline{c}$ Fock state is

$$\frac{dP_{\rm ic}^n}{dx_i \ldots dx_n} = N_n \alpha_s^4(M_{c\overline{c}}) \frac{\delta(1-\sum_{i=1}^n x_i)}{(m_h^2 - \sum_{i=1}^n (\widehat{m}_i^2/x_i))^2}, \tag{6}$$

where N_n normalizes the $|nc\overline{c}\rangle$ probability, $P_{\rm ic}^n$, and $n = 4$, 5 for meson and baryon production from the $|n_V c\overline{c}\rangle$ configuration. The delta function conserves longitudinal momentum. The dominant Fock configurations are closest to the light-cone energy shell and therefore the invariant mass, $M^2 = \sum_i \widehat{m}_i^2/x_i$, is minimized where $\widehat{m}_i^2 = k_{T,i}^2 + m_i^2$ is the effective transverse mass of the $i^{\rm th}$ particle and x_i is the light-cone momentum fraction. Assuming $\langle \boldsymbol{k}_{T,i}^2 \rangle$ is proportional to the square of the constituent quark mass, we choose $\widehat{m}_q = 0.45$ GeV, $\widehat{m}_s = 0.71$ GeV, and $\widehat{m}_c = 1.8$ GeV [16,17].

The intrinsic charm production cross section for a single charm hadron from the n-particle state can be related to $P_{\rm ic}^n$ and the inelastic hN cross section by

$$\sigma_{\rm ic}^n(hN) = P_{\rm ic}^n \sigma_{hN}^{\rm in} \frac{\mu^2}{4\widehat{m}_c^2}. \tag{7}$$

The factor of $\mu^2/4\widehat{m}_c^2$ arises from the soft interaction which breaks the coherence of the Fock state. To set the scale of the coherence factor μ we assume that the NA3 diffractive J/ψ cross section [35] can be attributed to intrinsic charm. In this experiment the nuclear dependence of J/ψ production in $\pi^- A$ interactions into a "hard" contribution with a nearly linear A dependence at low x_F and a high x_F "diffractive" contribution scaling as A^β where $\beta = 0.77$ for pion and 0.71 for proton beams, characteristic of soft interactions.

Then we assume that the diffractive fraction of the production cross section [35] is the same for charmonium and charm hadrons. In Ref. [11], $\mu^2 \sim 0.2$ GeV^2 was found. However, calculations with more recent parton densities suggest that $\mu^2 \sim 0.1$ GeV^2. We thus obtain $\sigma^4_{\rm ic}(\pi N) \approx 0.5$ μb and $\sigma^5_{\rm ic}(pN) \approx 0.7$ μb at 200 GeV. We take $P^5_{\rm ic} = 0.31\%$, as determined from an analysis of the EMC charm structure function data [36]. A recent reanalysis of the EMC data with next-to-leading-order calculations of leading-twist and intrinsic charm electroproduction is consistent with the presence of an intrinsic charm component in the proton at large $x_{\rm Bj}$ of $\approx 1\%$ or less [37]. For simplicity, we will always assume that the total probability for a charm quark in an $|n_V c\bar{c}\rangle$ state is 0.31% [36,37], regardless of the projectile identity.

The inelastic $\Sigma^- p$ cross section has not been measured. However, the total and elastic Λp cross sections have been parameterized for beam momenta less than 200 GeV albeit with large statistical uncertainties. Extrapolating these cross sections to 330 GeV, we found that $\sigma^{\rm in}_{\Lambda p} > \sigma^{\rm in}_{pp}$ at this energy which seems unlikely. To be conservative, we therefore scaled $\sigma^{\rm in}_{pp}$ to $\sigma^{\rm in}_{\Lambda p}$ at the highest measured Λp energy and used the energy dependence of $\sigma^{\rm in}_{pp}$ thereafter to set the scale for $\Sigma^- p$ interactions at larger values of $\sqrt{s}$.

There are two ways of producing charm hadrons from intrinsic $c\bar{c}$ states. The first is by uncorrelated fragmentation, previously discussed in Section 2. Additionally, if the projectile has the corresponding valence quarks, the charm quark can also hadronize by coalescence with the valence spectators. The coalescence mechanism thus introduces flavor correlations between the projectile and the final-state hadrons, producing e.g. Ξ_c^0's with a large fraction of the Σ^- momentum.

First we briefly discuss charm production by uncorrelated fragmentation. If we assume that the c quark fragments into a D meson, the D distribution is

$$\frac{dP^{nF}_{\rm ic}}{dx_D} = \int dz \prod_{i=1}^{n} dx_i \frac{dP^n_{\rm ic}}{dx_1 \ldots dx_n} D_{D/c}(z)\delta(x_D - z x_c) \,, \tag{8}$$

These distributions are assumed for all intrinsic charm production by uncorrelated fragmentation with $D_{H/c}(z) = \delta(z-1)$. We will not use Peterson function fragmentation further in this work.

The coalescence distributions, on the other hand, are specific for the individual charm hadrons. It is reasonable to assume that the intrinsic charm Fock states are fragile and can easily materialize into charm hadrons in high-energy, low momentum transfer reactions through coalescence. These contributions, taken from Ref. [14], do not include any binding energy of the produced hadrons or any mass effects. The coalescence contribution to charm hadron production is

$$\frac{dP^{nC}_{\rm ic}}{dx_H} = \int \prod_{i=1}^{n} dx_i \frac{dP^n_{\rm ic}}{dx_1 \ldots dx_n} \delta(x_H - x_{H_1} - \ldots - x_{H_{n_V}}) \,. \tag{9}$$

The coalescence function is simply a delta function combining the momentum fractions of the quarks in the Fock state configuration that make up the valence quarks of the final-state hadron.

Table 1
The lowest number of partons needed in an intrinsic charm Fock state configuration for the charm particle to be produced by coalescence. Note that 4 and 5 correspond to the minimal $|n_V c\bar{c}\rangle$ configuration while the higher states refer to $|n_V c\bar{c}d\bar{d}\rangle$, etc.

Particle	$\Sigma^-(dds)$	$p(uud)$	$\pi^-(\bar{u}d)$
$D^-(d\bar{c})$	5	5	4
$D^+(\bar{d}c)$	$7(d\bar{d})$	$7(d\bar{d})$	$6(d\bar{d})$
$\Lambda_c(udc)$	$7(u\bar{u})$	5	$6(u\bar{u})$
$\Sigma_c^0(ddc)$	5	$7(d\bar{d})$	$6(d\bar{d})$
$D_s^-(s\bar{c})$	5	$7(s\bar{s})$	$6(s\bar{s})$
$D_s^+(\bar{s}c)$	$7(s\bar{s})$	$7(s\bar{s})$	$6(s\bar{s})$
$\Xi_c^0(dsc)$	5	$7(s\bar{s})$	$6(s\bar{s})$
$\Xi_c^+(usc)$	$7(u\bar{u})$	$7(s\bar{s})$	$8(s\bar{s}u\bar{u})$

We now compare and contrast D^-, D^+, D_s^- and D_s^+ meson and Λ_c, Σ_c^0, Ξ_c^0 and Ξ_c^+ baryon production by coalescence from Σ^-, p and π^- projectiles. We note that not all of these hadrons can be produced from the minimal intrinsic charm Fock state configuration, $|n_V c\bar{c}\rangle$. However, coalescence can also occur within higher fluctuations of the intrinsic charm Fock state. For example, in the proton, the D^+ and Ξ_c^0 can be produced by coalescence from $|n_V c\bar{c}d\bar{d}\rangle$ and $|n_V c\bar{c}s\bar{s}\rangle$ configurations. These higher Fock state probabilities can be obtained using earlier results [12,38]. In a previous study of $\psi\psi$ production from $|n_V c\bar{c}c\bar{c}\rangle$ states [38] the double intrinsic charm production probability, $P_{\rm icc}$, was determined assuming that all the measured $\psi\psi$ pairs [39,40] arise from these configurations. The resulting upper bound on the model, $\sigma_{\psi\psi} = \sigma_{\rm ic}^{\psi\psi}(\pi^- N) \approx 20$ pb set by experiment [39], requires $P_{\rm icc} \approx 4.4\%\ P_{\rm ic}$ [38,41]. This value can then be used to estimate the probability of light quark pairs in an intrinsic charm state. We expect that the probability of additional light quark pairs in the Fock states to be larger than $P_{\rm icc}$,

$$P_{\rm icq} \approx \left(\frac{\widehat{m}_c}{\widehat{m}_q}\right)^2 P_{\rm icc}\,, \tag{10}$$

leading to $P_{\rm icu} = P_{\rm icd} \approx 70.4\%\ P_{\rm ic}$ and $P_{\rm ics} \approx 28.5\%\ P_{\rm ic}$. To go to still higher configurations, e.g. for Ξ_c^+ production from a π^-, one can make the similar assumption that $P_{\rm icsu} = 70.4\% P_{\rm ics}$.

In Table 1 we show the minimum number of partons needed in each configuration to produce a given charm hadron. When more than the minimal $|n_V c\bar{c}\rangle$ state is necessary for coalescence to occur, the additional light quark pairs required in the state are indicated. While we include the eight particle configuration necessary to produce a Ξ_c^+ by coalescence from a π^- projectile, we will confine our discussion to charm hadron production from the minimal state and states with one additional $q\bar{q}$ pair only.

The total intrinsic charm contribution to charm hadron production is a combination of uncorrelated fragmentation and coalescence. In previous works [11,12,16,17] only production by uncorrelated fragmentation from the minimal $|n_V c\bar{c}\rangle$ states and coalescence from the minimum Fock state configuration was considered. This was so because a significant leading effect is present only in the minimal configuration, i.e. there is

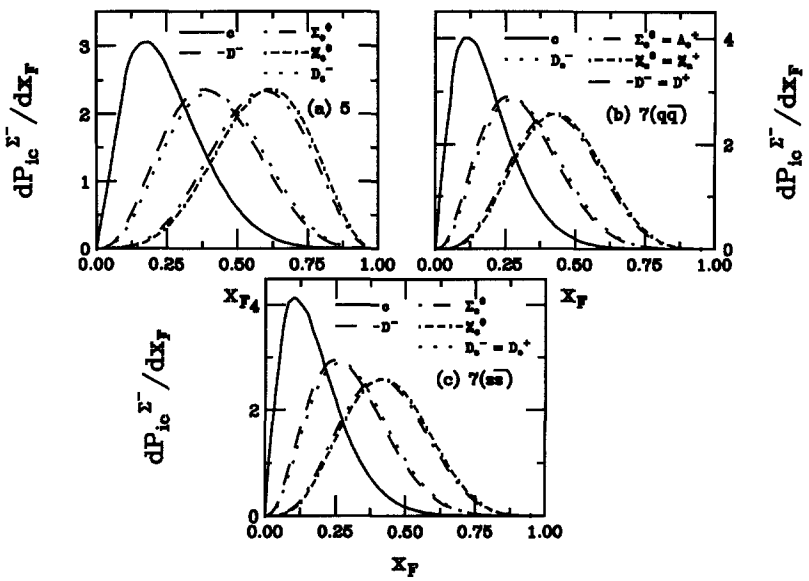

Fig. 4. Charm hadron production in the intrinsic charm model with a Σ^- projectile. The probability distributions, $(1/P_{\rm ic}^n)(dP_{\rm ic}^n/dx_H)$, for uncorrelated fragmentation and coalescence are given for the minimal 5-particle Fock state (a) and for the 7-particle Fock states with light quarks $q = u, d$ (b) and with strange quarks (c). The solid curve in each case is the charm quark distribution which also serves as the hadron distribution for independent fragmentation. The other curves are the probability distributions for hadron production by coalescence, including: D^- (dashed), Σ_c^0 (dot-dashed), Ξ_c^0 (dot-dash-dashed) and D_s^- (dotted). If the shape of the probability distribution is the same for any two hadrons (such as the Σ_c^0 and the Λ_c^+ in (b)) in a configuration, it is indicated.

no difference between D^+ and D^- mesons produced from $|n_V c\bar{c}d\bar{d}\rangle$ states. Also, as more partons are included in the Fock state, the coalescence distributions soften and approach the fragmentation distributions, eventually producing charm hadrons with less momentum than uncorrelated fragmentation from the minimal $c\bar{c}$ state if a sufficient number of $q\bar{q}$ pairs are included. There is then no longer any advantage to introducing more light quark pairs into the configuration—the relative probability will decrease while the potential gain in momentum is not significant. However, if some fraction of the final-state hadrons are assumed to be produced from higher Fock configurations, then all possible final states from those configurations should also be included. Therefore in this paper, we consider production by fragmentation and coalescence from the minimal state and the next higher states with $u\bar{u}$, $d\bar{d}$ and $s\bar{s}$ pairs.

The probability distributions, $(1/P_{\rm ic}^n)(dP_{\rm ic}^n/dx_H)$, are given in Figs. 4–6 for Σ^-, p and π^- projectiles respectively. It is clear from Fig. 4 that the Σ^- projectile allows the greatest coalescence production of charm hadrons from the minimal Fock configuration, Fig. 4a. The charm baryons are quite fast, taking more than 50% of the projectile momentum. The difference between charm and charm-strange hadron production is very small due to the strange and light quark mass difference. Because the strange quark is more massive, it carries a somewhat larger fraction of the Σ^- momentum than the light quarks, resulting in a slightly larger average momentum for the Ξ_c^0 and the D_s^-

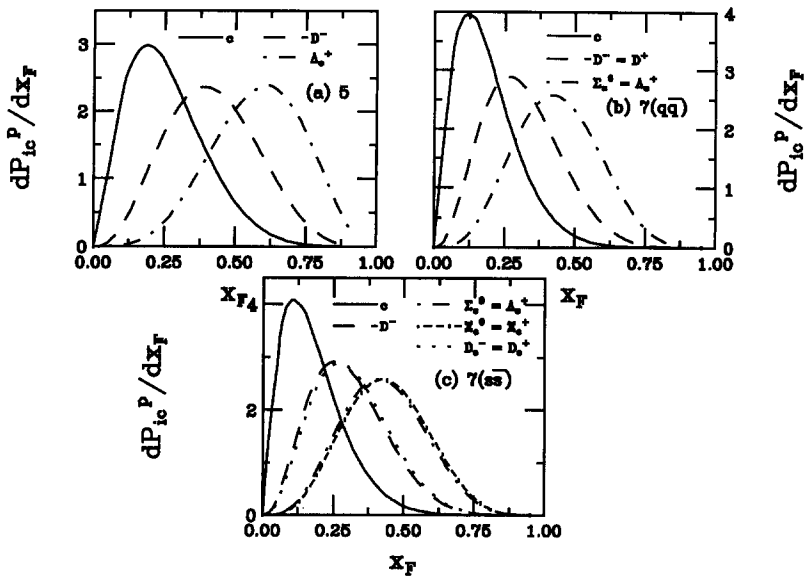

Fig. 5. Charm hadron production in the intrinsic charm model with a proton projectile. The probability distributions, $(1/P_{ic}^{n})(dP_{ic}^{n}/dx_H)$, for uncorrelated fragmentation and coalescence are given for the minimal 5-particle Fock state (a) and for the 7-particle Fock states with light quarks $q = u, d$ (b) and with strange quarks (c). The solid curve in each case is the charm quark distribution which also serves as the hadron distribution for independent fragmentation. The other curves are the probability distributions for hadron production by coalescence, including: D^- (dashed), Λ_c^+ (dot-dashed), Ξ_c^0 (dot-dash-dashed) and D_s^- (dotted). If the shape of the probability distribution is the same for any two hadrons (such as the Σ_c^0 and the Λ_c^+ in (b)) in a configuration, it is indicated.

relative to the Σ_c^0 and D^-, on the order of 3–4%, as can be seen in Table 2. The c quark distribution itself, leading to uncorrelated fragmentation, carries $\approx 25\%$ of the projectile momentum in the minimal state. This is reduced by $\approx 35\%$ in the seven-particle Fock configurations. In this model, the c and $\bar{c}$ probability distributions are identical. We note that these higher configurations can produce, for example, Σ_c^0 and Λ_c baryons from $|n_V c\bar{c}d\bar{d}\rangle$ and $|n_V c\bar{c}u\bar{u}\rangle$ states respectively with the same probability distribution, shown in Fig. 4b, but not necessarily with the same relative probability, as we will show shortly. Introducing an $s\bar{s}$ pair to the 7-particle configuration reduces the average momentum of the final-state hadron by $\approx 2\%$ over the average in the 7-particle configurations with lighter $q\bar{q}$ pairs. In addition to the reduction of the average momentum of the c quark in the higher configurations, the final-state charm hadron momentum from this configuration is reduced as well, suggesting that no more significant contribution to the overall momentum of the final hadron will be obtained by including yet higher Fock configurations.

While fewer charm hadrons can be directly produced from the minimal configuration of a proton projectile, as evident from Fig. 5, their average momentum is somewhat higher than the Σ^- due to the absence of the strange valence quark. However, this only affects the final-state average momentum by 1–2%. Final-state charm hadrons from a pion projectile, shown in Fig. 6 have, on average, 20% more momentum than from a

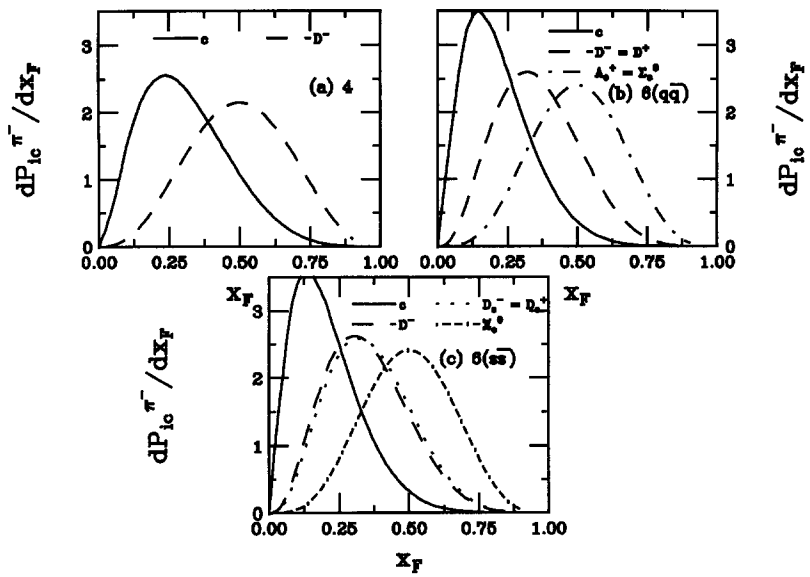

Fig. 6. Charm hadron production in the intrinsic charm model with a π^- projectile. The probability distributions, $(1/P_{\rm ic}^n)(dP_{\rm ic}^n/dx_H)$, for uncorrelated fragmentation and coalescence are given for the minimal 5-particle Fock state (a) and for the 7-particle Fock states with light quarks $q = u$, d (b) and with strange quarks (c). The solid curve in each case is the charm quark distribution which also serves as the hadron distribution for independent fragmentation. The other curves are the probability distributions for hadron production by coalescence, including: D^- (dashed), Λ_c^+ (dot-dashed), Ξ_c^0 (dot-dash-dashed) and D_s^- (dotted). If the shape of the probability distribution is the same for any two hadrons (such as the Σ_c^0 and the Λ_c^+ in (b)) in a configuration, it is indicated.

baryon projectile because the total velocity is shared between fewer initial partons. Note also that mesons from a four-particle Fock configuration and baryons from a six-particle Fock state each receive half of the projectile momentum.

4. Model predictions

We now turn to specific predictions of our model. We begin with the x_F distribution of the final-state charm hadrons. The x_F distribution for final-state hadron H is the sum of the leading-twist fusion and intrinsic charm components,

$$\frac{d\sigma_{hN}^H}{dx_F} = \frac{d\sigma_{\rm lt}^H}{dx_F} + \frac{d\sigma_{\rm ic}^H}{dx_F}\,, \tag{11}$$

where $d\sigma_{\rm ic}^H/dx_F$ is related to dP_H/dx_F by

$$\frac{d\sigma_{\rm ic}^H}{dx_F} = \sigma_{hN}^{\rm in}\frac{\mu^2}{4\widehat{m}_c^2}\frac{dP_H}{dx_F}\,. \tag{12}$$

The probability distribution is the sum of all contributions from the $|n_V c\bar{c}\rangle$ and the $|n_V c\bar{c}q\bar{q}\rangle$ configurations with $q = u$, d, and s and includes uncorrelated fragmentation

Table 2
The average value of x_F for charm particles produced by coalescence from Σ^-, p and π^- projectiles in $|n_V c\bar{c}\rangle$, $|n_V c\bar{c}q\bar{q}\rangle$ and $|n_V c\bar{c}s\bar{s}\rangle$ states. In this case, $q\bar{q} = u\bar{u}$, $d\bar{d}$.

State	Particle	$\Sigma^-(n_V = dds)$	$p(n_V = uud)$	$\pi^-(n_V = \bar{u}d)$
$\|n_V c\bar{c}\rangle$	c	0.251	0.256	0.308
	$D^-(d\bar{c})$	0.41	0.419	0.499
	$\Lambda_c(udc)$	–	0.58	–
	$\Sigma_c^0(ddc)$	0.573	–	–
	$D_s^-(s\bar{c})$	0.427	–	–
	$\Xi_c^0(dsc)$	0.59	–	–
$\|n_V c\bar{c}q\bar{q}\rangle$	c	0.185	0.188	0.219
	$D^-(d\bar{c}) = D^+(\bar{d}c)$	0.31	0.314	0.359
	$\Lambda_c(udc)$	0.433	0.438	0.5
	$\Sigma_c^0(ddc)$	0.433	0.438	0.5
	$D_s^-(s\bar{c})$	0.32	–	–
	$\Xi_c^0(dsc) = \Xi_c^+(usc)$	0.444	–	–
$\|n_V c\bar{c}s\bar{s}\rangle$	c	0.179	0.181	0.211
	$D^-(d\bar{c})$	0.302	0.306	0.349
	$\Lambda_c(udc)$	–	0.429	–
	$\Sigma_c^0(ddc)$	0.424	–	–
	$D_s^-(s\bar{c}) = D_s^+(\bar{s}c)$	0.312	0.316	0.361
	$\Xi_c^0(dsc)$	0.434	0.439	0.5
	$\Xi_c^+(usc)$	0.434	–	–

and coalescence when appropriate, as described below. We use the same fragmentation function, either the delta or Peterson function, to calculate uncorrelated fragmentation in both leading-twist fusion and intrinsic charm. In this section, we use only the delta function.

Since experimental information on the relative rates of charm hadron production is incomplete, we assume that all the lowest lying charm hadrons produced by uncorrelated fragmentation have equal probability in both leading-twist fusion and intrinsic charm. There are ten charm hadrons—and the same number of anticharm hadrons—if excited charm hadrons such as D^* and $\Lambda_c^+(2593)$ are excluded. Therefore the probability distribution for uncorrelated fragmentation into each of these hadrons is 10% of the total probability. As can be seen in Table 1, only a fraction of the possible final-state hadrons can be produced by coalescence. We use a simple counting scheme to arrive at the coalescence probability which enhances the production of leading charm at large x_F. We note that the combined probability of fragmentation and coalescence of all charm hadrons cannot exceed the total production probability of the Fock state configuration. Thus when a particular final-state hadron can be produced both by uncorrelated fragmentation and coalescence, we multiply the sum of the fragmentation and coalescence probabilities by 0.5 to keep the total probability fixed.

As a concrete example of how the total probability distributions of charm hadron production from the intrinsic charm model is calculated, we will describe D^+ and D^- production from the Σ^- beam in our model in detail. The full complement of equations

for all the final-state charm hadrons from Σ^-, p and π^- projectiles considered in this work can be found in Appendix A. In the $|ddsc\bar{c}\rangle$ configuration, there are four final-state hadrons with a valence c quark ($2\Xi_c^0$, Σ_c^0 and J/ψ) and also four final-state hadrons with a valence $\bar{c}$ quark ($2D^-$, D_s^- and J/ψ). Note that the J/ψ has been counted in each category. The D^- is then produced by coalescence with 50% of the total coalescence probability for hadrons with a valence $\bar{c}$ as well as by uncorrelated fragmentation of the $\bar{c}$ while the D^+ is only produced by uncorrelated fragmentation from this state. The probability distributions from this minimal Fock configuration are then

$$\frac{dP^5_{D^-}}{dx_F} = \frac{1}{2}\left(\frac{1}{10}\frac{dP^{5F}_{\rm ic}}{dx_F} + \frac{1}{2}\frac{dP^{5C}_{\rm ic}}{dx_F}\right), \tag{13}$$

$$\frac{dP^5_{D^+}}{dx_F} = \frac{1}{10}\frac{dP^{5F}_{\rm ic}}{dx_F}, \tag{14}$$

where F refers to uncorrelated fragmentation and C to coalescence into the specific final state with the associated probability distribution, shown in Fig. 4a. The $|ddsc\bar{c}q\bar{q}\rangle$ configurations where $q\bar{q} = u\bar{u}$, $d\bar{d}$ and $s\bar{s}$ allow coalescence production of eight final-state hadrons with a valence c and five final-state hadrons with a valence $\bar{c}$ in each case. We will discuss D^+ and D^- from each of these configurations in turn. When $q\bar{q} = u\bar{u}$, the possible hadrons produced by coalescence are: $2\Xi_c^+$, Ξ_c^0, $2\Lambda_c^+$, Σ_c^0, D^0 and J/ψ with a valence c and $2D^-$, D_s^-, $\overline{D}^0$ and J/ψ with a valence $\bar{c}$. A final state D^+ can be produced by coalescence from the $d\bar{d}$ configuration in one of the eight possible final-state hadrons with a valence c quark ($3\Sigma_c^0$, $3\Xi_c^0$, D^+ and J/ψ) while the D^- is produced by coalescence in three out of five combinations ($3D^-$, D_s^- and J/ψ) with a valence $\bar{c}$. The $s\bar{s}$ configuration yields no D^+ by coalescence—$4\Xi_c^0$, Σ_c^0, $\Omega_c^0(ssc)$, D_s^+ and J/ψ are allowed—while $2D^-$ are allowed out of five possible hadrons with valence $\bar{c}$ quarks—$2D^-$, $2D_s^-$ and J/ψ. Finally, the total intrinsic charm probability distribution for these mesons is:

$$\begin{aligned}\frac{dP_{D^-}}{dx_F} = {} & \frac{1}{2}\left(\frac{1}{10}\frac{dP^{5F}_{\rm ic}}{dx_F} + \frac{1}{2}\frac{dP^{5C}_{\rm ic}}{dx_F}\right) + \frac{1}{2}\left(\frac{1}{10}\frac{dP^{7F}_{\rm icu}}{dx_F} + \frac{2}{5}\frac{dP^{7C}_{\rm icu}}{dx_F}\right) \\ & + \frac{1}{2}\left(\frac{1}{10}\frac{dP^{7F}_{\rm icd}}{dx_F} + \frac{3}{5}\frac{dP^{7C}_{\rm icd}}{dx_F}\right) + \frac{1}{2}\left(\frac{1}{10}\frac{dP^{7F}_{\rm ics}}{dx_F} + \frac{2}{5}\frac{dP^{7C}_{\rm ics}}{dx_F}\right),\end{aligned} \tag{15}$$

$$\frac{dP_{D^+}}{dx_F} = \frac{1}{10}\frac{dP^{5F}_{\rm ic}}{dx_F} + \frac{1}{10}\frac{dP^{7F}_{\rm icu}}{dx_F} + \frac{1}{2}\left(\frac{1}{10}\frac{dP^{7F}_{\rm icd}}{dx_F} + \frac{1}{8}\frac{dP^{7C}_{\rm icd}}{dx_F}\right) + \frac{1}{10}\frac{dP^{7F}_{\rm ics}}{dx_F}. \tag{16}$$

Lastly we note that only fragmentation from the minimal Fock state was included along with coalescence from the lowest possible configuration in earlier work [11,12,17]. This corresponds to the first term of the D^- probability distribution while the D^+ distribution would be proportional to $0.5(\frac{1}{10}dP^{5F}_{\rm ic}/dx_F + \frac{1}{8}dP^{7C}_{\rm icd}/dx_F)$.

We must also account for the fact that most of the data are taken on nuclear targets. In this case, the model assumes a linear A dependence for leading-twist fusion and an A^α dependence for the intrinsic charm component [35] where $\alpha = 0.77$ for pions and 0.71 for protons (and Σ^-)

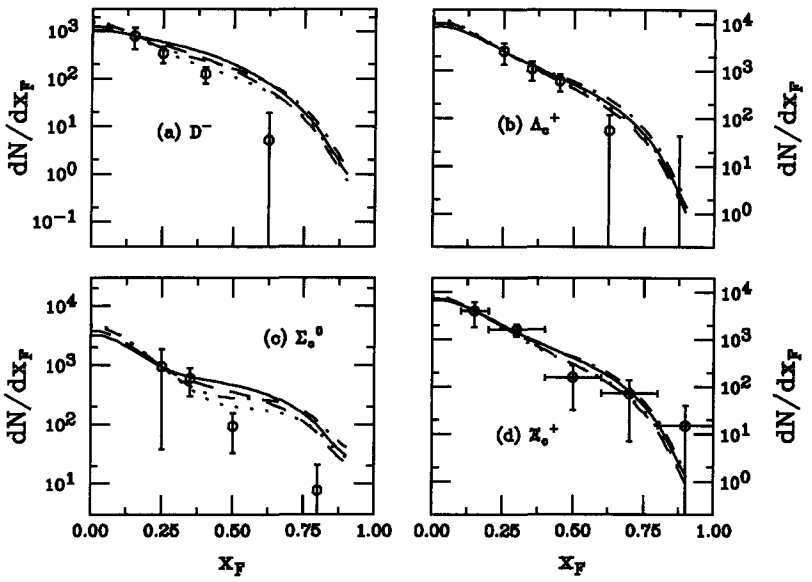

Fig. 7. Model predictions are compared to the $\Sigma^- A$ data of Ref. [8] for (a) D^-, (b) Λ_c^+, (c) Σ_c^0 and (d) Ξ_c^+. The solid and dashed curves represent our full model, with the intrinsic charm probability distributions given in Eqs. (A.1)–(A.8) for carbon and copper targets respectively. The dot-dashed and dotted curves contrast the results for carbon and copper targets respectively with the simplified model which considers only fragmentation from the minimal Fock state and coalescence only from the state with the minimum number of partons necessary to produce it.

$$\frac{d\sigma_{hA}^H}{dx_F} = A\frac{d\sigma_{\rm lt}^H}{dx_F} + A^\alpha \frac{d\sigma_{\rm ic}^H}{dx_F}. \tag{17}$$

This A dependence is included in the calculations. The intrinsic charm contribution to the longitudinal momentum distributions per nucleon is thus reduced for nuclear targets.

We now compare the model calculations, both the full model of Eqs. (15) and (16) and the simpler model used previously, to the WA89 data [8] on carbon and copper targets in Fig. 7. Since the data are unnormalized, we have normalized all curves to the first data point. The dot-dashed and dotted curves are results with the previous simplified model [11,12,17] on carbon and copper targets respectively. The full model is illustrated in the solid and dashed curves for the same targets. The agreement with the data is quite reasonable given both the low statistics of the data and our normalization to the first data point rather than fitting the normalization to the data. The differences in the model distributions are most obvious for the Σ_c^0, shown in Fig. 7c. The simpler model emphasizes the coalescence production from the $|n_V c\bar{c}\rangle$ state only. As can be seen from Fig. 4 and Table 2, the average x_F of the coalescence distribution is more than a factor of two larger than that of a Σ_c^0 production by independent fragmentation of a c quark, producing a shoulder in the x_F distribution, particularly for the carbon target (dot-dashed curve). Because the Σ_c^0 is produced by coalescence with $\approx 30\%$ less average momentum from the 7-particle Fock states, the intermediate x_F region is partially filled in, resulting in a smoother x_F distribution even though the probability

Table 3
The average value of x_F for charm particles produced in the full model for Σ^-, p and π^- projectiles on a copper target. The model results are given at 330 GeV and 650 GeV for Σ^-Cu interactions, 650 GeV for π^-Cu interactions and 800 GeV for pCu interactions. For comparison, the average from PYTHIA at $x_F > 0$ in each case is also shown.

This Model				
Particle	Σ^-Cu (330)	Σ^-Cu (650)	π^-Cu (650)	pCu (800)
$D^-(d\bar{c})$	0.192	0.147	0.169	0.120
$D^+(\bar{d}c)$	0.133	0.112	0.152	0.107
$\Lambda_c(udc)$	0.145	0.118	0.154	0.146
$\Sigma_c^0(ddc)$	0.187	0.140	0.154	0.107
$D_s^-(s\bar{c})$	0.165	0.129	0.151	0.106
$D_s^+(\bar{s}c)$	0.132	0.111	0.151	0.105
$\Xi_c^0(dsc)$	0.221	0.160	0.151	0.106
$\Xi_c^+(usc)$	0.160	0.126	0.150	0.106
PYTHIA				
Particle	Σ^-p (330)	Σ^-p (650)	π^-p (650)	pp (800)
$D^-(d\bar{c})$	0.14	0.126	0.254	0.113
$D^+(\bar{d}c)$	0.18	0.159	0.173	0.160
$\Lambda_c(udc)$	0.54	0.468	0.153	0.604
$\Sigma_c^0(ddc)$	0.72	0.707	0.146	0.35
$D_s^-(s\bar{c})$	0.155	0.139	0.172	0.097
$D_s^+(\bar{s}c)$	0.171	0.154	0.16	0.153
$\Xi_c^0(dsc)$	0.76	0.767	0.157	0.123
$\Xi_c^+(usc)$	0.55	0.477	0.156	0.155

is reduced for the higher Fock states. Similar results can be seen for the other charm hadrons in Fig. 7.

Note that the model results are in much better agreement with the data than the PYTHIA simulations at the same energy with the default settings, shown in Fig. 1c,d. If the PYTHIA predictions are superimposed on Fig. 7 with the same normalization as our model, the PYTHIA results would considerably exceed the data at large x_F for the charm baryons. In particular, since the c quark is pulled forward by a valence dd diquark, the Σ_c^0 rate from PYTHIA at $x_F \approx 0.8$ would exceed the data by nearly four orders of magnitude. The differences in the results are also obvious in Table 3 where the average x_F of all the model distributions on a copper target are compared to PYTHIA calculations with a proton target at the same energy.

Another way to quantify leading charm production is through the asymmetry between leading and non-leading charm. The asymmetry is defined as

$$A(x_F) = \frac{d\sigma_L/dx_F - d\sigma_{NL}/dx_F}{d\sigma_L/dx_F + d\sigma_{NL}/dx_F}, \tag{18}$$

where L represents the leading and NL the non-leading charm hadron. High statistics

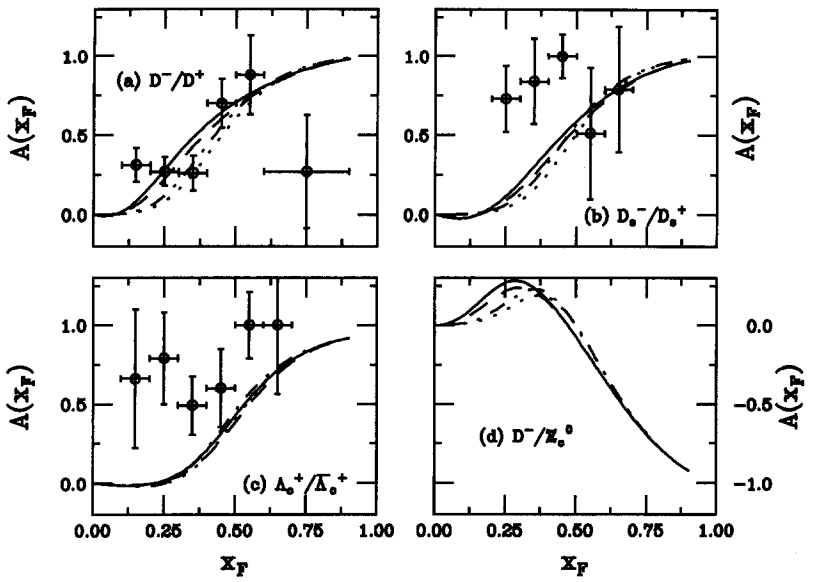

Fig. 8. Model predictions are compared to the $\Sigma^- A$ data of Ref. [9] for the following asymmetries: (a) D^-/D^+, (b) D_s^-/D_s^+ and (c) $\Lambda_c^+/\overline{\Lambda}_c^+$, as well as our prediction for the (d) D^-/Ξ_c^0 asymmetry. The solid and dashed curves represent our full model, with the intrinsic charm probability distributions given in Eqs. (A.1)-(A.8) for carbon and copper targets respectively. The dot-dashed and dotted curves for carbon and copper targets respectively contrast the results with the simplified model which considers only fragmentation from the minimal Fock state and coalescence only from the state with the minimum number of partons necessary to produce it.

data has previously been available only from π^- beams where a significant enhancement of D^- over D^+ production was seen at $x_F > 0.3$ [1,4,5], in qualitative agreement with the intrinsic charm calculation of Ref. [11]. The model [12] also correctly predicted the symmetric production of D_s^- and D_s^+ mesons and Λ_c^+ and $\overline{\Lambda}_c^+$ baryons by π^- beams [7,32,42].

Statistics are unfortunately limited on charm production by baryon beams. Recently the WA89 collaboration has presented the D^-/D^+, D_s^-/D_s^+ and $\Lambda_c^+/\overline{\Lambda}_c^+$ asymmetries from their Σ^- data [9]. In Fig. 8 we compare our calculations with both models to this data as well as show a prediction for the asymmetry between the D^- and Ξ_c^0, both of which are produced from the partons of the minimal Fock configuration. The full model gives a larger asymmetry between D^- and D^+ at low x_F than the simpler assumptions of previous work [11,12] because D^- production at intermediate x_F is enhanced by coalescence production from the 7-particle configurations, see also Fig. 7a. Our results with the full model are in qualitative agreement with the data, shown in Fig. 8a. The measured D_s^-/D_s^+ and $\Lambda_c^+/\overline{\Lambda}_c^+$ asymmetries are larger than our predictions at intermediate x_F. The probability distribution for $\overline{\Lambda}_c^+$ in our model is

$$\frac{dP_{\overline{\Lambda}_c^+}}{dx_F} = \frac{1}{10}\frac{dP_{\rm ic}^{4F}}{dx_F} + \frac{1}{10}\frac{dP_{\rm icu}^{6F}}{dx_F} + \frac{1}{10}\frac{dP_{\rm icd}^{6F}}{dx_F} + \frac{1}{10}\frac{dP_{\rm ics}^{6F}}{dx_F}. \tag{19}$$

Some of the discrepancies between the model and the data may arise from the relatively

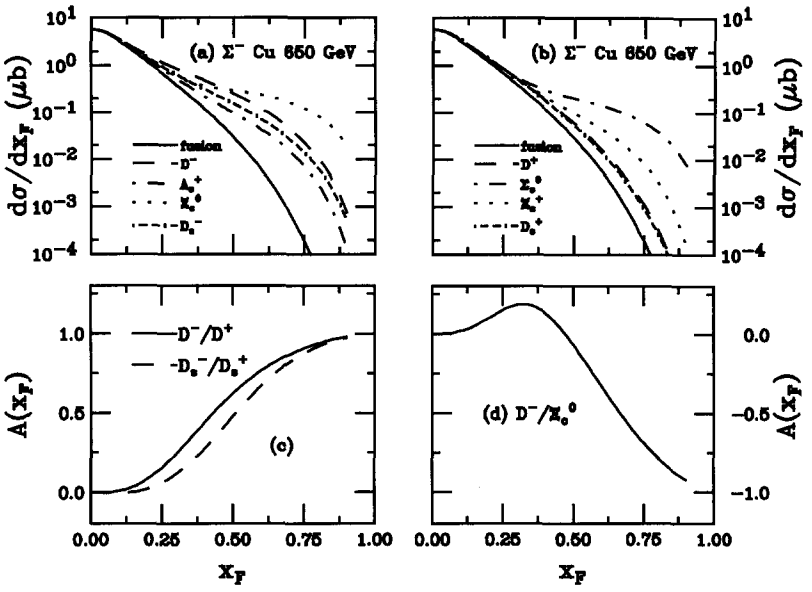

Fig. 9. Predictions for charm hadron production are given in our full model for Σ^-Cu interactions at 650 GeV. The individual x_F distributions are given in (a) and (b). All cross sections are compared to the leading-twist fusion calculation in the solid curve. In (a) the hadron distributions are D^- (dashed), Λ_c^+ (dot-dashed), Ξ_c^0 (dotted) and D_s^- (dot-dashed-dashed). In (b) the hadron distributions are D^+ (dashed), Σ_c^0 (dot-dashed), Ξ_c^+ (dotted) and D_s^+ (dot-dashed-dashed). Predictions of the asymmetries are given in (c) for D^-/D^+ (solid) and D_s^-/D_s^+ (dashed) while the prediction for the D^-/Ξ_c^0 asymmetry is given in (d).

low statistics of the D_s and Λ_c measurements. Our model is also quite crude in overall normalization for the different final states since we assume that all final-state hadrons are produced by independent fragmentation with the same probability. Not enough high statistics data exist yet for us to use experimental absolute production rates as a guide. The asymmetry between D^- and Ξ_c^0 is interesting because the $|ddsc\bar{c}\rangle$ state of the Σ^- can be thought of as a virtual $D^-\Xi_c^0$ fluctuation, as has been suggested for proton fluctuations into $K^+\Lambda$ [43,44] and $D^-\Lambda_c^+$ [44]. The D^-/Ξ_c^0 asymmetry is positive at first since the D^- x_F distribution is larger at intermediate x_F, especially when the 7-particle configurations are included. At larger x_F, the baryon distributions always lead over charm mesons produced in the same configuration, causing the D^-/Ξ_c^0 asymmetry to approach -1 as $x_F \to 1$. Similar results should be expected from the models of Refs. [43,44].

We now turn to predictions of charm hadron production at SELEX with 650 GeV beams of Σ^- and π^- [10]. First we give the charm hadron x_F distributions for Σ^-Cu interactions and the relevant asymmetries in Fig. 9. Since the leading-twist fusion cross section grows faster than σ_{ic}^H, the average x_F of the particles studied decreases $\approx 30\%$ from 330 GeV to 650 GeV. A smaller decrease is found from the PYTHIA model, showing the relative strength of the string fragmentation mechanism, as can be seen in Table 3. The Ξ_c^0 is clearly the hardest distribution, followed by the Σ_c^0. The Ξ_c^0 leads the Σ_c^0 because the more massive valence s quark carries more of the Σ^- velocity

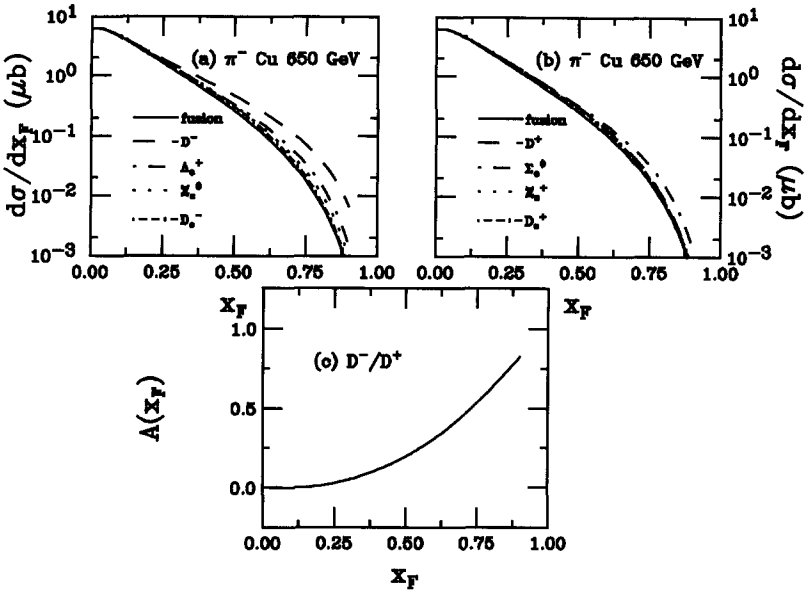

Fig. 10. Predictions for charm hadron production are given in our full model for 650 GeV π^-Cu interactions. The individual x_F distributions are given in (a) and (b). All cross sections are compared to the leading-twist fusion calculation in the solid curve. In (a) the hadron distributions are D^- (dashed), Λ_c^+ (dot-dashed), Ξ_c^0 (dotted) and D_s^- (dot-dashed-dashed). In (b) the hadron distributions are D^+ (dashed), Σ_c^0 (dot-dashed), Ξ_c^+ (dotted) and D_s^+ (dot-dashed-dashed). A prediction of the D^-/D^+ asymmetry is given in (c).

than the d valence quarks. The Ξ_c^+ leads the Λ_c^+ in the 7-particle $u\bar{u}$ state for the same reason. The D^- and D_s^-, also produced from the 5-particle state have the hardest meson distributions but lag the baryons. The D^+ and D_s^+ have the softest distributions with the D^+ slightly harder because the quarks in the $d\bar{d}$ configuration get slightly more velocity than the $s\bar{s}$ configuration with the more massive strange quarks. The asymmetries, which should be compared to the dashed curves in Fig. 8, are somewhat reduced at higher energies, again due to the larger leading-twist cross section.

Since SELEX will also measure charm hadroproduction with a π^- beam at the same energy, these predictions are shown in Fig. 10. Because only the D^- is produced from the minimal Fock state configuration, it shows the hardest x_F distribution in Fig. 10a. Note that since $c\bar{c}$ production by leading-twist fusion alone is already significantly harder than the equivalent production by baryon projectiles, the distributions produced by coalescence from 6-particle configurations are not substantially enhanced over the fusion cross section, even at large x_F. The intrinsic charm cross section is proportional to $\sigma_{\pi N}^{\rm in}$ which increases slowly compared to the leading-twist cross section, further decreasing the predicted leading charm enhancement. Additionally, we note that charm baryons lead mesons produced by coalescence only in the 6-particle configurations since the baryons take $\approx 50\%$ of the pion momentum while the mesons take less, as seen in Fig. 6 and Table 2. The PYTHIA distributions in Fig. 3, aside from the leading D^-, are more central, also evident from Table 3. In Fig. 10c, only the D^-/D^+ asymmetry is shown because the model predicts identical D_s^- and D_s^+ meson and Λ_c and $\overline{\Lambda_c^+}$ baryon

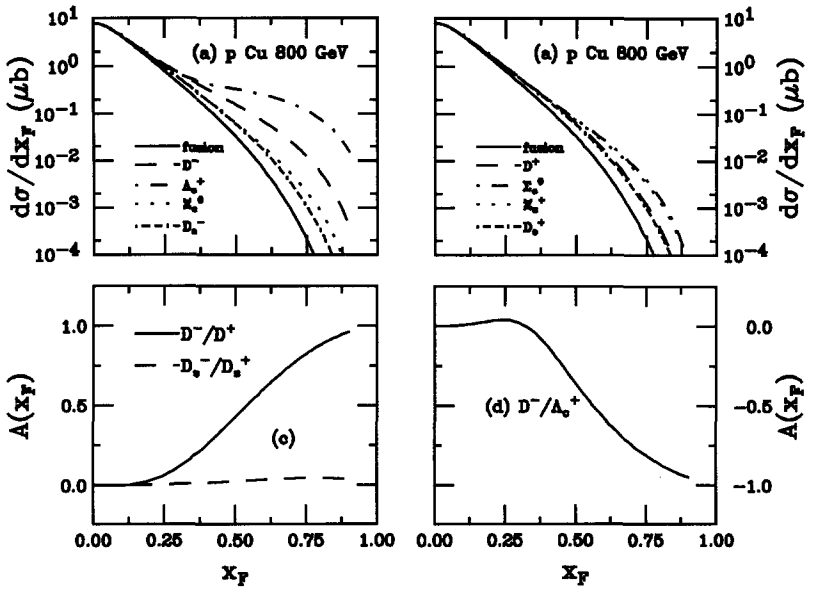

Fig. 11. Predictions for charm hadron production are given in our full model for pCu interactions at 800 GeV. The individual x_F distributions are given in (a) and (b). All cross sections are compared to the leading-twist fusion calculation in the solid curve. In (a) the hadron distributions are D^- (dashed), Λ_c^+ (dot-dashed), Ξ_c^0 (dotted) and D_s^- (dot dashed dashed). In (b) the hadron distributions are D^+ (dashed), Σ_c^0 (dot-dashed), Ξ_c^+ (dotted) and D_s^+ (dot dashed dashed). Predictions of the asymmetries are given in (c) for D^-/D^+ (solid) and D_s^-/D_s^+ (dashed) while the prediction for the D^-/Λ_c^+ asymmetry is given in (d).

distributions, see Appendix A, hence no asymmetry. We note that the asymmetry is reduced compared to calculations at lower energy [11].

The primary proton beam for fixed-target experiments at Fermilab is 800 GeV so for completeness, we also give predictions for a possible pA measurement at this energy in Fig. 11. In this case, the Λ_c^+ has the hardest x_F distribution followed by the D^-, both of which are produced by coalescence from the 5-particle Fock state. Again, the Σ_c^0 and D^+ are somewhat harder than the Ξ_c^+ and D_s^+ distributions respectively due to the relative partitioning of the parton velocity in the 7-particle $u\bar{u}$ and $d\bar{d}$ configurations compared to the 7-particle $s\bar{s}$ state. The model predicts a strong D^-/D^+ asymmetry as well as a D^-/Λ_c^+ asymmetry, comparable to the D^-/Ξ_c^0 asymmetry predicted for the $\Sigma^- A$ interactions. On the other hand, the D_s^-/D_s^+ asymmetry is quite weak. Such measurements with a proton beam would provide a useful complement to a high statistics Σ^- measurement. A comprehensive understanding of data with proton projectiles has suffered in the past from a lack of statistics and high precision proton data, compared to that from Σ^- and π^- projectiles, could eliminate certain models.

5. Summary and conclusions

We have refined the intrinsic charm model of Refs. [11,12,17], including both the minimal Fock state and all the configurations with an additional $q\bar{q}$ pair. We have applied a simple counting scheme to determine the relative contribution of each state to the final charm hadron distribution. The model compares rather favorably to the x_F distributions measured by WA89 [8] and produces reasonable agreement with their measured D^-/D^+ asymmetry while falling short of the D_s^-/D_s^+ and $\Lambda_c/\overline{\Lambda}_c$ data [9] at intermediate x_F.

Further, we have made predictions for charm hadron production at the energy of SELEX for both Σ^- and π^- projectiles. Predictions for production by an 800 GeV proton beam are also given. High statistics data on charm production from a combination of these projectiles could eliminate certain classes of models and perhaps distinguish between coalescence in the initial state, as in the intrinsic charm model, and in the final state, as in models such as PYTHIA [18]. The simple counting scheme employed here could be replaced with relative rates from data. However, the shapes of the distributions would not change significantly in our model. Therefore a collection of charm production data could define the role of intrinsic charm in future experiments.

Acknowledgements

We thank S.J. Brodsky, E. Ramberg, H.-W. Siebert and T. Sjöstrand for discussions.

Appendix A

Here we give the probability distributions for D^-, D^+, D_s^- and D_s^+ mesons and Λ_c^+, Σ_c^0, Ξ_c^0 and Ξ_c^+ baryons for production by the minimal and first three higher Fock state configurations from Σ^-, proton and π^- projectiles. The probability distributions for each final state are given in Figs. 4–6. We note that the predictions for Λ_c^+ and Σ_c^+ are identical in all cases because their quark content is the same. Recall that $P_{\rm ic}^5 = 0.31\%$, $P_{\rm icu}^7 = P_{\rm icd}^7 = 70.4\%\ P_{\rm ic}^5$ and $P_{\rm ics}^7 = 28.5\%\ P_{\rm ic}^5$.

We begin with the Σ^-. In the $|ddsc\bar{c}\rangle$ configuration, there are four final-state hadrons with a valence c quark ($2\Xi_c^0$, Σ_c^0 and J/ψ) and also four final-state hadrons with a valence $\bar{c}$ quark ($2D^-$, D_s^- and J/ψ). The $|ddsc\bar{c}q\bar{q}\rangle$ configurations where $q\bar{q} = u\bar{u}$, $d\bar{d}$ and $s\bar{s}$ allow coalescence production of eight possible final-state hadrons with a valence c and five possible final-state hadrons with a valence $\bar{c}$. When $q\bar{q} = u\bar{u}$, the possible hadrons produced by coalescence are $2\Xi_c^+$, Ξ_c^0, $2\Lambda_c^+$, Σ_c^0, D^0 and J/ψ with a valence c and $2D^-$, D_s^-, $\overline{D}^0$ and J/ψ with a valence $\bar{c}$. The $d\bar{d}$ configuration allows coalescence production of the following hadrons with a valence c quark, $3\Sigma_c^0$, $3\Xi_c^0$, D^+ and J/ψ, and, with a valence $\bar{c}$, $3D^-$, D_s^- and J/ψ. The $s\bar{s}$ configuration yields $4\Xi_c^0$,

Σ_c^0, $\Omega_c^0(ssc)$, D_s^+ and J/ψ while the final-state valence $\bar{c}$ quarks hadrons are $2D^-$, $2D_s^-$ and J/ψ. We have

$$\frac{dP_{D^-}}{dx_F} = \frac{1}{2}\left(\frac{1}{10}\frac{dP_{\rm ic}^{5F}}{dx_F} + \frac{1}{2}\frac{dP_{\rm ic}^{5C}}{dx_F}\right) + \frac{1}{2}\left(\frac{1}{10}\frac{dP_{\rm icu}^{7F}}{dx_F} + \frac{2}{5}\frac{dP_{\rm icu}^{7C}}{dx_F}\right) + \frac{1}{2}\left(\frac{1}{10}\frac{dP_{\rm icd}^{7F}}{dx_F} + \frac{3}{5}\frac{dP_{\rm icd}^{7C}}{dx_F}\right) + \frac{1}{2}\left(\frac{1}{10}\frac{dP_{\rm ics}^{7F}}{dx_F} + \frac{2}{5}\frac{dP_{\rm ics}^{7C}}{dx_F}\right), \tag{A.1}$$

$$\frac{dP_{D^+}}{dx_F} = \frac{1}{10}\frac{dP_{\rm ic}^{5F}}{dx_F} + \frac{1}{10}\frac{dP_{\rm icu}^{7F}}{dx_F} + \frac{1}{2}\left(\frac{1}{10}\frac{dP_{\rm icd}^{7F}}{dx_F} + \frac{1}{8}\frac{dP_{\rm icd}^{7C}}{dx_F}\right) + \frac{1}{10}\frac{dP_{\rm ics}^{7F}}{dx_F}, \tag{A.2}$$

$$\frac{dP_{\Lambda_c^+}}{dx_F} = \frac{1}{10}\frac{dP_{\rm ic}^{5F}}{dx_F} + \frac{1}{2}\left(\frac{1}{10}\frac{dP_{\rm icu}^{7F}}{dx_F} + \frac{1}{4}\frac{dP_{\rm icu}^{7C}}{dx_F}\right) + \frac{1}{10}\frac{dP_{\rm icd}^{7F}}{dx_F} + \frac{1}{10}\frac{dP_{\rm ics}^{7F}}{dx_F}, \tag{A.3}$$

$$\frac{dP_{\Sigma_c^0}}{dx_F} = \frac{1}{2}\left(\frac{1}{10}\frac{dP_{\rm ic}^{5F}}{dx_F} + \frac{1}{4}\frac{dP_{\rm ic}^{5C}}{dx_F}\right) + \frac{1}{2}\left(\frac{1}{10}\frac{dP_{\rm icu}^{7F}}{dx_F} + \frac{1}{8}\frac{dP_{\rm icu}^{7C}}{dx_F}\right) + \frac{1}{2}\left(\frac{1}{10}\frac{dP_{\rm icd}^{7F}}{dx_F} + \frac{3}{8}\frac{dP_{\rm icd}^{7C}}{dx_F}\right) + \frac{1}{2}\left(\frac{1}{10}\frac{dP_{\rm ics}^{7F}}{dx_F} + \frac{1}{8}\frac{dP_{\rm ics}^{7C}}{dx_F}\right), \tag{A.4}$$

$$\frac{dP_{D_s^-}}{dx_F} = \frac{1}{2}\left(\frac{1}{10}\frac{dP_{\rm ic}^{5F}}{dx_F} + \frac{1}{4}\frac{dP_{\rm ic}^{5C}}{dx_F}\right) + \frac{1}{2}\left(\frac{1}{10}\frac{dP_{\rm icu}^{7F}}{dx_F} + \frac{1}{5}\frac{dP_{\rm icu}^{7C}}{dx_F}\right) + \frac{1}{2}\left(\frac{1}{10}\frac{dP_{\rm icd}^{7F}}{dx_F} + \frac{1}{5}\frac{dP_{\rm icd}^{7C}}{dx_F}\right) + \frac{1}{2}\left(\frac{1}{10}\frac{dP_{\rm ics}^{7F}}{dx_F} + \frac{2}{5}\frac{dP_{\rm ics}^{7C}}{dx_F}\right), \tag{A.5}$$

$$\frac{dP_{D_s^+}}{dx_F} = \frac{1}{10}\frac{dP_{\rm ic}^{5F}}{dx_F} + \frac{1}{10}\frac{dP_{\rm icu}^{7F}}{dx_F} + \frac{1}{10}\frac{dP_{\rm icd}^{7F}}{dx_F} + \frac{1}{2}\left(\frac{1}{10}\frac{dP_{\rm ics}^{7F}}{dx_F} + \frac{1}{8}\frac{dP_{\rm ics}^{7C}}{dx_F}\right), \tag{A.6}$$

$$\frac{dP_{\Xi_c^0}}{dx_F} = \frac{1}{2}\left(\frac{1}{10}\frac{dP_{\rm ic}^{5F}}{dx_F} + \frac{1}{2}\frac{dP_{\rm ic}^{5C}}{dx_F}\right) + \frac{1}{2}\left(\frac{1}{10}\frac{dP_{\rm icu}^{7F}}{dx_F} + \frac{1}{8}\frac{dP_{\rm icu}^{7C}}{dx_F}\right) + \frac{1}{2}\left(\frac{1}{10}\frac{dP_{\rm icd}^{7F}}{dx_F} + \frac{3}{8}\frac{dP_{\rm icd}^{7C}}{dx_F}\right) + \frac{1}{2}\left(\frac{1}{10}\frac{dP_{\rm ics}^{7F}}{dx_F} + \frac{1}{2}\frac{dP_{\rm ics}^{7C}}{dx_F}\right), \tag{A.7}$$

$$\frac{dP_{\Xi_c^+}}{dx_F} = \frac{1}{10}\frac{dP_{\rm ic}^{5F}}{dx_F} + \frac{1}{2}\left(\frac{1}{10}\frac{dP_{\rm icu}^{7F}}{dx_F} + \frac{1}{4}\frac{dP_{\rm icu}^{7C}}{dx_F}\right) + \frac{1}{10}\frac{dP_{\rm icd}^{7F}}{dx_F} + \frac{1}{10}\frac{dP_{\rm ics}^{7F}}{dx_F}. \tag{A.8}$$

Fewer charm hadrons are produced by coalescence from the five-quark configuration of the proton since it has no valence strange quark. In the $|uudc\bar{c}\rangle$ configuration, there are four final-state hadrons with a valence c quark ($2\Lambda_c^+$, $\Sigma_c^{++}(uuc)$ and J/ψ) and also four final-state hadrons with a valence $\bar{c}$ quark ($2\overline{D}^0$, D^- and J/ψ). The $|uudc\bar{c}q\bar{q}\rangle$ configurations allow coalescence production of eight possible final-state hadrons with a valence c and five possible final-state hadrons with a valence $\bar{c}$. When $q\bar{q} = u\bar{u}$, the possible hadrons produced by coalescence are $3\Lambda_c^+$, $3\Sigma_c^{++}$, D^0 and J/ψ with a valence c and D^-, $3\overline{D}^0$ and J/ψ with a valence $\bar{c}$. The $d\bar{d}$ configuration allows coalescence production of the following hadrons with a valence c quark, $4\Lambda_c^+$, Σ_c^0, Σ_c^{++}, D^+ and J/ψ, and, with a valence $\bar{c}$, $2D^-$, $2\overline{D}^0$ and J/ψ. The $s\bar{s}$ configuration yields $2\Xi_c^+$, Ξ_c^0, $2\Lambda_c^+$, Σ_c^{++}, D_s^+ and J/ψ while the final-state valence $\bar{c}$ quarks hadrons are $2D^-$, $\overline{D}^0$, D_s^- and J/ψ. Then

$$\frac{dP_{D^-}}{dx_F} = \frac{1}{2}\left(\frac{1}{10}\frac{dP_{\rm ic}^{5F}}{dx_F} + \frac{1}{4}\frac{dP_{\rm ic}^{5C}}{dx_F}\right) + \frac{1}{2}\left(\frac{1}{10}\frac{dP_{\rm icu}^{7F}}{dx_F} + \frac{1}{5}\frac{dP_{\rm icu}^{7C}}{dx_F}\right) + \frac{1}{2}\left(\frac{1}{10}\frac{dP_{\rm icd}^{7F}}{dx_F} + \frac{2}{5}\frac{dP_{\rm icd}^{7C}}{dx_F}\right) + \frac{1}{2}\left(\frac{1}{10}\frac{dP_{\rm ics}^{7F}}{dx_F} + \frac{1}{5}\frac{dP_{\rm ics}^{7C}}{dx_F}\right), \tag{A.9}$$

$$\frac{dP_{D^+}}{dx_F} = \frac{1}{10}\frac{dP_{\rm ic}^{5F}}{dx_F} + \frac{1}{10}\frac{dP_{\rm icu}^{7F}}{dx_F} + \frac{1}{2}\left(\frac{1}{10}\frac{dP_{\rm icd}^{7F}}{dx_F} + \frac{1}{8}\frac{dP_{\rm icd}^{7C}}{dx_F}\right) + \frac{1}{10}\frac{dP_{\rm ics}^{7F}}{dx_F}, \tag{A.10}$$

$$\frac{dP_{\Lambda_c^+}}{dx_F} = \frac{1}{2}\left(\frac{1}{10}\frac{dP_{\rm ic}^{5F}}{dx_F} + \frac{1}{2}\frac{dP_{\rm ic}^{5C}}{dx_F}\right) + \frac{1}{2}\left(\frac{1}{10}\frac{dP_{\rm icu}^{7F}}{dx_F} + \frac{3}{8}\frac{dP_{\rm icu}^{7C}}{dx_F}\right) + \frac{1}{2}\left(\frac{1}{10}\frac{dP_{\rm icd}^{7F}}{dx_F} + \frac{1}{2}\frac{dP_{\rm icd}^{7C}}{dx_F}\right) + \frac{1}{2}\left(\frac{1}{10}\frac{dP_{\rm ics}^{7F}}{dx_F} + \frac{1}{4}\frac{dP_{\rm ics}^{7C}}{dx_F}\right), \tag{A.11}$$

$$\frac{dP_{\Sigma_c^0}}{dx_F} = \frac{1}{10}\frac{dP_{\rm ic}^{5F}}{dx_F} + \frac{1}{10}\frac{dP_{\rm icu}^{7F}}{dx_F} + \frac{1}{2}\left(\frac{1}{10}\frac{dP_{\rm icd}^{7F}}{dx_F} + \frac{1}{8}\frac{dP_{\rm icd}^{7C}}{dx_F}\right) + \frac{1}{10}\frac{dP_{\rm ics}^{7F}}{dx_F}, \tag{A.12}$$

$$\frac{dP_{D_s^-}}{dx_F} = \frac{1}{10}\frac{dP_{\rm ic}^{5F}}{dx_F} + \frac{1}{10}\frac{dP_{\rm icu}^{7F}}{dx_F} + \frac{1}{10}\frac{dP_{\rm icd}^{7F}}{dx_F} + \frac{1}{2}\left(\frac{1}{10}\frac{dP_{\rm ics}^{7F}}{dx_F} + \frac{1}{5}\frac{dP_{\rm ics}^{7C}}{dx_F}\right), \tag{A.13}$$

$$\frac{dP_{D_s^+}}{dx_F} = \frac{1}{10}\frac{dP_{\rm ic}^{5F}}{dx_F} + \frac{1}{10}\frac{dP_{\rm icu}^{7F}}{dx_F} + \frac{1}{10}\frac{dP_{\rm icd}^{7F}}{dx_F} + \frac{1}{2}\left(\frac{1}{10}\frac{dP_{\rm ics}^{7F}}{dx_F} + \frac{1}{8}\frac{dP_{\rm ics}^{7C}}{dx_F}\right), \tag{A.14}$$

$$\frac{dP_{\Xi_c^0}}{dx_F} = \frac{1}{10}\frac{dP_{\rm ic}^{5F}}{dx_F} + \frac{1}{10}\frac{dP_{\rm icu}^{7F}}{dx_F} + \frac{1}{10}\frac{dP_{\rm icd}^{7F}}{dx_F} + \frac{1}{2}\left(\frac{1}{10}\frac{dP_{\rm ics}^{7F}}{dx_F} + \frac{1}{8}\frac{dP_{\rm ics}^{7C}}{dx_F}\right), \tag{A.15}$$

$$\frac{dP_{\Xi_c^+}}{dx_F} = \frac{1}{10}\frac{dP_{\rm ic}^{5F}}{dx_F} + \frac{1}{10}\frac{dP_{\rm icu}^{7F}}{dx_F} + \frac{1}{10}\frac{dP_{\rm icd}^{7F}}{dx_F} + \frac{1}{2}\left(\frac{1}{10}\frac{dP_{\rm ics}^{7F}}{dx_F} + \frac{1}{4}\frac{dP_{\rm ics}^{7C}}{dx_F}\right). \tag{A.16}$$

Charm and anticharm hadron production is more symmetric from the π^- because the projectile contains a valence antiquark of its own. In the minimal $|\overline{u}dc\overline{c}\rangle$ configuration, there are two possible final-state hadrons with a valence c quark (D^0 and J/ψ) and also two possible final-state hadrons with a valence $\overline{c}$ quark (D^- and J/ψ). The $|\overline{u}dc\overline{c}q\overline{q}\rangle$ configurations allow coalescence production of four possible final-state hadrons with a valence c and likewise four possible final-state hadrons with a valence $\overline{c}$. When $q\overline{q} = u\overline{u}$, the possible hadrons produced by coalescence are: Λ_c^+, $2D^0$ and J/ψ with a valence c and D^-, $\overline{D}^0$, $\overline{\Sigma}_c^{++}$ and J/ψ with a valence $\overline{c}$. The $d\overline{d}$ configuration allows coalescence production of the following hadrons with a valence c quark, Σ_c^0, D^0, D^+ and J/ψ, and, with a valence $\overline{c}$, D^-, $\overline{D}^0$, $\overline{\Lambda}_c^+$ and J/ψ. The $s\overline{s}$ configuration yields Ξ_c^0, D_s^+, D^0 and J/ψ with a valence c while the possible final-state valence $\overline{c}$ quarks hadrons are D^-, D_s^-, $\overline{\Xi}_c^+$ and J/ψ. In this case

$$\frac{dP_{D^-}}{dx_F} = \frac{1}{2}\left(\frac{1}{10}\frac{dP_{\rm ic}^{4F}}{dx_F} + \frac{1}{2}\frac{dP_{\rm ic}^{4C}}{dx_F}\right) + \frac{1}{2}\left(\frac{1}{10}\frac{dP_{\rm icu}^{6F}}{dx_F} + \frac{1}{4}\frac{dP_{\rm icu}^{6C}}{dx_F}\right) + \frac{1}{2}\left(\frac{1}{10}\frac{dP_{\rm icd}^{6F}}{dx_F} + \frac{1}{2}\frac{dP_{\rm icd}^{6C}}{dx_F}\right) + \frac{1}{2}\left(\frac{1}{10}\frac{dP_{\rm ics}^{6F}}{dx_F} + \frac{1}{4}\frac{dP_{\rm ics}^{6C}}{dx_F}\right), \tag{A.17}$$

$$\frac{dP_{D^+}}{dx_F} = \frac{1}{10}\frac{dP_{\rm ic}^{4F}}{dx_F} + \frac{1}{10}\frac{dP_{\rm icu}^{6F}}{dx_F} + \frac{1}{2}\left(\frac{1}{10}\frac{dP_{\rm icd}^{6F}}{dx_F} + \frac{1}{4}\frac{dP_{\rm icd}^{6C}}{dx_F}\right) + \frac{1}{10}\frac{dP_{\rm ics}^{6F}}{dx_F}, \tag{A.18}$$

$$\frac{dP_{\Lambda_c^+}}{dx_F} = \frac{1}{10}\frac{dP_{\rm ic}^{4F}}{dx_F} + \frac{1}{2}\left(\frac{1}{10}\frac{dP_{\rm icu}^{6F}}{dx_F} + \frac{1}{4}\frac{dP_{\rm icu}^{6C}}{dx_F}\right) + \frac{1}{10}\frac{dP_{\rm icd}^{6F}}{dx_F} + \frac{1}{10}\frac{dP_{\rm ics}^{6F}}{dx_F}, \tag{A.19}$$

$$\frac{dP_{\Sigma_c^0}}{dx_F} = \frac{1}{10}\frac{dP_{\rm ic}^{4F}}{dx_F} + \frac{1}{10}\frac{dP_{\rm icu}^{6F}}{dx_F} + \frac{1}{2}\left(\frac{1}{10}\frac{dP_{\rm icd}^{6F}}{dx_F} + \frac{1}{4}\frac{dP_{\rm icd}^{6C}}{dx_F}\right) + \frac{1}{10}\frac{dP_{\rm ics}^{6F}}{dx_F}, \tag{A.20}$$

$$\frac{dP_{D_s^-}}{dx_F} = \frac{1}{10}\frac{dP_{\rm ic}^{4F}}{dx_F} + \frac{1}{10}\frac{dP_{\rm icu}^{6F}}{dx_F} + \frac{1}{10}\frac{dP_{\rm icd}^{6F}}{dx_F} + \frac{1}{2}\left(\frac{1}{10}\frac{dP_{\rm ics}^{6F}}{dx_F} + \frac{1}{4}\frac{dP_{\rm ics}^{6C}}{dx_F}\right), \tag{A.21}$$

$$\frac{dP_{D_s^+}}{dx_F} = \frac{1}{10}\frac{dP_{\rm ic}^{4F}}{dx_F} + \frac{1}{10}\frac{dP_{\rm icu}^{6F}}{dx_F} + \frac{1}{10}\frac{dP_{\rm icd}^{6F}}{dx_F} + \frac{1}{2}\left(\frac{1}{10}\frac{dP_{\rm ics}^{6F}}{dx_F} + \frac{1}{4}\frac{dP_{\rm ics}^{6C}}{dx_F}\right), \tag{A.22}$$

$$\frac{dP_{\Xi_c^0}}{dx_F} = \frac{1}{10}\frac{dP_{\rm ic}^{4F}}{dx_F} + \frac{1}{10}\frac{dP_{\rm icu}^{6F}}{dx_F} + \frac{1}{10}\frac{dP_{\rm icd}^{6F}}{dx_F} + \frac{1}{2}\left(\frac{1}{10}\frac{dP_{\rm ics}^{6F}}{dx_F} + \frac{1}{4}\frac{dP_{\rm ics}^{6C}}{dx_F}\right), \tag{A.23}$$

$$\frac{dP_{\Xi_c^+}}{dx_F} = \frac{1}{10}\frac{dP_{\rm ic}^{4F}}{dx_F} + \frac{1}{10}\frac{dP_{\rm icu}^{6F}}{dx_F} + \frac{1}{10}\frac{dP_{\rm icd}^{6F}}{dx_F} + \frac{1}{10}\frac{dP_{\rm ics}^{6F}}{dx_F}. \tag{A.24}$$

References

[1] E.M. Aitala et al. (E791 Collab.), Phys. Lett. B 371 (1996) 157.
[2] M. Aguilar-Benitez et al. (LEBC-EHS Collab.), Phys. Lett. B 161 (1985) 400; Z. Phys. C 31 (1986) 491.
[3] S. Barlag et al. (ACCMOR Collab.), Z. Phys. C 49 (1991) 555.
[4] M.I. Adamovich et al. (WA82 Collab.), Phys. Lett. B 305 (1993) 402.
[5] G.A. Alves et al. (E769 Collab.), Phys. Rev. Lett. 72 (1994) 812.
[6] J.C. Collins, D.E. Soper and G. Sterman, Perturbative QCD, ed. A.H. Mueller (World Scientific, Singapore, 1989);
G. Bodwin, Phys. Rev. D 31 (1985) 2616; D 34 (1986) 3932;
J. Qiu and G. Sterman, Nucl. Phys. B 353 (1991) 105, 137.
[7] E.M. Aitala et al. (E791 Collab.), Phys. Lett. B 411 (1997) 230.
[8] R. Werding (WA89 Collab.), *in* Proc. of *ICHEP94*, 27th Int. Conf. on High Energy Physics, Glasgow, Scotland (1994).
[9] M.I. Adamovich et al. (WA89 Collab.), CERN-EP/98-41.
[10] E. Ramberg, *in* Hyperons, Charm and Beauty Hadrons, Proc. of the 2nd Int. Conf. on Hyperons, Charm and Beauty Hadrons, Montreal, Canada, 1996, ed. C.S. Kalman et al., Nucl. Phys. B (Proc. Suppl.) 55 A (1997) 173.
[11] R. Vogt and S.J. Brodsky, Nucl. Phys. B 438 (1995) 261.
[12] R. Vogt and S.J. Brodsky, Nucl. Phys. B 478 (1996) 311.
[13] S.J. Brodsky, J.F. Gunion and D.E. Soper, Phys. Rev. D 36 (1987) 2710.
[14] S.J. Brodsky, P. Hoyer, C. Peterson and N. Sakai, Phys. Lett. B 93 (1980) 451;
S. J. Brodsky, C. Peterson and N. Sakai, Phys. Rev. D 23 (1981) 2745.
[15] S.J. Brodsky, P. Hoyer, A.H. Mueller and W.-K. Tang, Nucl. Phys. B 369 (1992) 519.
[16] R. Vogt, S.J. Brodsky and P. Hoyer, Nucl. Phys. B 360 (1991) 67.
[17] R. Vogt, S.J. Brodsky and P. Hoyer, Nucl. Phys. B 383 (1992) 643.
[18] T. Sjöstrand, Comput. Phys. Commun. 82 (1994) 74. Program updates and documentation can be found at http://www.thep.lu.se/tf2/staff/torbjorn/Pythia.html.
[19] R.C. Hwa, Phys. Rev. D 27 (1983) 653; Oregon preprint OITS-539 (1994).
[20] V.A. Bednyakov, Dubna preprint JINR E2-94-79 (1994), hep-ph/9403270;
V.G. Kartvelishvili, A.K. Likhoded and S.R. Slobospitskii, Sov. J. Nucl. Phys. 33 (1981) 434 [Yad. Fiz. 33 (1981) 832].
[21] R. Vogt, Z. Phys. C 71 (1996) 475.
[22] S. Frixione, M.L. Mangano, P. Nason and G. Ridolfi, Nucl. Phys. B 431 (1994) 453.
[23] R.K. Ellis, *in* Physics at the 100 GeV Scale, Proc. of the 17th SLAC Summer Institute, Stanford, CA, 1989, ed. E.C. Brennan (SLAC Report No. 361) 45.

[24] M. Glück, E. Reya, A. Vogt, Z. Phys. C 67 (1995) 433.
[25] A.D. Martin, R.G. Roberts and W.J. Stirling, Phys. Lett. B 306 (1993) 145.
[26] M. Glück, E. Reya, and A. Vogt, Z. Phys. C 53 (1992) 651.
[27] P.J. Sutton, A.D. Martin, R.G. Roberts and W.J. Stirling, Phys. Rev. D 45 (1992) 2349.
[28] C. Peterson, D. Schlatter, I. Schmitt, and P. Zerwas, Phys. Rev. D 27 (1983) 105.
[29] J. Chirn, *in* Proc. of the Int. Symp. on the Production and Decay of Heavy Flavors, Stanford, CA, ed. E. Bloom and A. Fridman (1987) p. 131.
[30] M. Aguilar-Benitez et al. (LEBC-EHS Collab.), Phys. Lett. B189 (1987) 476.
[31] M. Aguilar-Benitez et al. (LEBC-EHS Collab.), Phys. Lett. B 161 (1985) 400; Z. Phys. C 31 (1986) 491.
[32] S. Barlag et al. (ACCMOR Collab.), Phys. Lett. B 247 (1990) 113.
[33] T. Sjöstrand, private communication.
[34] P. Hoyer and S.J. Brodsky, *in* Proc. of the Topical Conf. on Particle Production Near Threshold, Nashville, IN, ed. H. Hann and E.J. Stephenson (1990) 238.
[35] J. Badier et al. (NA3 Collab.), Z. Phys. C 20 (1983) 101.
[36] J.J. Aubert et al. (EMC Collab.), Phys. Lett. B 110 (1982) 73;
E. Hoffmann and R. Moore, Z. Phys. C 20 (1983) 71.
[37] B.W. Harris, J. Smith and R. Vogt, Nucl. Phys. B 461 (1996) 181.
[38] R. Vogt and S.J. Brodsky, Phys. Lett. B 349 (1995) 569.
[39] J. Badier et al. (NA3 Collab.), Phys. Lett. B 114 (1982) 457.
[40] J. Badier et al. (NA3 Collab.), Phys. Lett. B 158 (1985) 85.
[41] R. Vogt, Nucl. Phys. B 446 (1995) 159.
[42] M.I. Adamovich et al. (BEATRICE Collab.), Nucl. Phys. B 495 (1997) 3.
[43] B.-Q. Ma and S.J. Brodsky, *in* Proc. of the ICTP Conf. on Perspectives in Hadronic Physics, Trieste, 1997, hep-ph/9707408.
[44] S. Paiva et al., IFUSP-P-1240, hep-ph/9610310.